Inorganic Chemistry

Article

pubs.acs.org/IC

Cubane-Type $Mo_3FeS_4{}^{4+,5+}$ Complexes Containing Outer Diphosphane Ligands: Ligand Substitution Reactions, Spectroscopic Studies, and Electronic Structure

Ivan Sorribes,[†] Francesc Lloret,[§] Joao C. Waerenborgh,[∥] Victor Polo,[⊥,#] Rosa Llusar,[*,†] and Cristian Vicent[*,‡]

[†]Departament de Química Física i Analítica and [‡]Serveis Centrals d'Instrumentació Cientifica, Universitat Jaume I, Av. Sos Baynat s/n, E- 12071 Castelló, Spain

[§]ICMOL-Universitat de Valencia, Spain

[∥]IST/ITN, Instituto Superior Técnico, Univ Tecnica de Lisboa, CFMC-UL, P-2686-953 Sacavém, Portugal

[⊥]Departamento de Química Física, Facultad de Ciencias, Universidad de Zaragoza, 50009 Zaragoza, Spain

[#]Instituto de Biocomputación y Física de Sistemas Complejos (BIFI), Universidad de Zaragoza, Mariano Esquillor s/n, 50018 Zaragoza, Spain

Ⓢ *Supporting Information*

ABSTRACT: A general protocol to access $Mo_3FeS_4{}^{4+}$ clusters selectively modified at the Fe coordination site is presented starting from the all-chlorine $Mo_3(FeCl)S_4(dmpe)_3Cl_3$ (**1**) [dmpe = 1,2-bis-(dimethylphosphane-ethane)] cluster and tetrabutylammonium salts (*n*-Bu_4NX) (X = CN^-, $N_3{}^-$, and PhS^-). Clusters $Mo_3(FeX)S_4(dmpe)_3Cl_3$ [X = CN^- (**2**), $N_3{}^-$ (**3**), and PhS^- (**4**)] are prepared in high yield, and comparison of geometric and redox features upon modification of the coordination environment at the Fe site at parity of ligands at the Mo sites is also presented. The existence of the cubane-type $Mo_3FeS_4{}^{4+,5+}$ redox couple is demonstrated by cyclic voltammetry and for compound **1** by cluster synthesis and X-ray structure determinations. Ground states for the **1**/**1**$^+$ redox couple are evaluated on the basis of magnetic susceptibility measurements, electron paramagnetic resonance, and ^{57}Fe Mössbauer spectroscopy aimed at providing an input of experimental data for electronic structure determination based on density functional theory calculations.

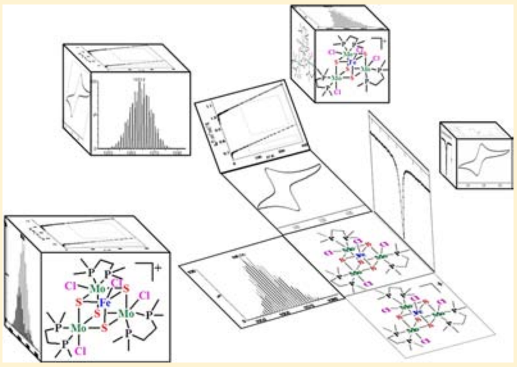

INTRODUCTION

Heterobimetallic cubane-type $MoFe_3S_4$ clusters, where the metal and sulfur atoms occupy adjacent vertices in a cube, have been extensively investigated in relation to metalloprotein systems.[1] Synthetic $MoFe_3S_4$ clusters serve as compositional and/or topological analogues of nitrogenase MoFe protein (that is, the nitrogen-fixing Fe–Mo cofactor that contains a $MoFe_7S_9$ core).[1b] In this context, for a wide spectrum of $MoFe_3S_4$ clusters,[2] nitrogenase-like catalysis as well as spectroscopic, structural, and electronic characteristics[1b] have been thoroughly investigated in view to fully understand multielectron reaction chemistry mediated by polynuclear Mo/Fe/S clusters occurring in nature.[3]

Another category of heterometal cubane-type compounds comprises the Mo_3MS_4 (M = transition or post-transition metal) complexes.[4] A series of $[Mo_3(MCl)S_4(dmpe)_3Cl_3]^{n+}$ (M = Fe, Co, Ni, Cu; *n* = 0, 1) compounds have been obtained in our group in which diphosphane and chlorine ligands fill the octahedral coordination environment of the Mo sites and chlorine ligands fill the outer tetrahedral position of the M atom (see Scheme 1). Except for M = Co, this family of compounds features fixed metal electron counts. Scheme 1 lists charge states of the complexes and metal electron counting along the isostructural $[Mo_3(MCl)S_4(dmpe)_3Cl_3]^{n+}$ (M = Fe, Co, Ni, Cu) series.

During our studies, we have found uses for them in catalysis for M = Ni,[5] Cu,[6] and nonlinear optics for M = Cu.[7] For M = Co, the isolation in substance of the first $Mo_3CoS_4{}^{4+,5+}$ redox couple has been achieved.[8] Recently, we have expanded our scope beyond these metals to include iron,[9] where kinetics of reaction and intimate mechanism operating for its substitutional lability at both the Fe and the Mo sites have been investigated providing a comparative group to Fe_4S_4 and $MoFe_3S_4$ clusters.

For the families of cubane-type Fe_4S_4 and $MoFe_3S_4$ clusters, their ability to reversibly accept and release electrons and understanding of their redox characteristics are of importance

Received: February 17, 2012
Published: September 25, 2012

Scheme 1

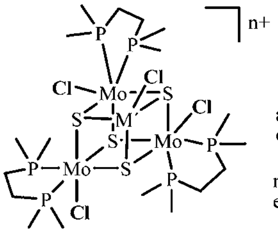

M′	Fe (n = 0)	Co (n = 0, 1)	Ni (n = 0)	Cu (n = 1)
accesible oxidation state	$Mo_3FeS_4^{4+}$	$Mo_3CoS_4^{4+,5+}$	$Mo_3NiS_4^{4+}$	$Mo_3CuS_4^{5+}$
metal electron counting	14	15, 14	16	16

from a fundamental perspective, and it is well documented that the accessibility of different redox states in these $MoFe_3S_4$ (and Fe_4S_4) clusters is dramatically affected by the choice of the peripheral ligands attached at the Fe sites. For this reason, developing well-defined synthetic entries for substitutional lability studies both at the Mo or at the Fe sites is of great importance. However, for Mo_3FeS_4 compounds, substitutional lability studies at the Fe site, isolation in substance, and detailed spectroscopic data of electron transfer series remain unknown. All Mo_3FeS_4 derivatives reported up to date, namely, $[Mo_3(FeH_2O)S_4(H_2O)_9](pts)_4$,[10] $[Mo_3(FeH_2O)S_4(NH_3)_9]Cl_4$,[11] $Mo_3(FeX)S_4Tp_3$ (X = Cl, Br) (Tp = hydrotris(pyrazolyl)borate),[12] $Cp_3'Mo_3(FeSH)S_4$ (Cp′ is MeCp),[13] the $[Mo_3(FeCl)S_4(H_2O)_8Cl]^{2+}$ dication,[14] and $Mo_3(FeCl)S_4(dmpe)_3Cl_3$[9] are invariably isolated as 14 metal electron species.[10,11] Moreover, for compound $Mo_3(FeCl)S_4(dmpe)_3Cl_3$,[9] physicochemical properties, other than crystal structures and kinetics of reaction toward NaSPh, have been incompletely examined. In particular, there has been no information on the range of accessible oxidation levels, magnetic properties, and ^{57}Fe Mössbauer spectroscopy and structures in different oxidation states, issues that are addressed in the present work.

Herein, we describe the ligand substitution reactions to generate a series of cubane-type $Mo_3(FeX)S_4(dmpe)_3Cl_3$ [dmpe =1,2-bis(dimethylphosphane-ethane); X = Cl (**1**), CN^- (**2**), N_3^- (**3**), and PhS^- (**4**)] clusters. We also present a structural study of the oxidized $\mathbf{1}^+$ cluster complex. Our results set the stage for a systematic exploration of the accessible electron transfer series as well as structural, spectroscopic, electronic, and magnetic properties upon varying the heterometal coordination environment and the metal electron counting. The understanding of such observed phenomena can be further improved by means of accurate density functional theory (DFT)[15] calculations, which provide direct information about changes on the geometrical parameters or the localization of unpaired spin density obtained from the analysis of the electronic structure for the experimentally studied $Mo_3FeS_4^{4+,5+}$ redox couples.

■ EXPERIMENTAL SECTION

Physical Measurements. Elemental analysis was carried out on a EuroEA3000 Eurovector Analyzer. Electrospray ionization (ESI) mass spectra were recorded on a Q-TOF Premier (quadrupole-T-wave-time-of-flight) instrument. A capillary voltage of 3.5 KV was used in the positive scan mode, and the cone voltage (U_c) was set to 15 V to control the extent of fragmentation of the identified ions. The chemical composition of each peak was assigned by comparison of the isotope experimental pattern with that calculated using the MassLynx 4.1 program. IR spectra were recorded in the 400−3500 cm^{-1} range on a Perkin-Elmer System 2000 FT-IR using KBr pellets. Cyclic voltammetry experiments were performed with a Echochemie Pgstat 20 electrochemical analyzer. All measurements were carried out with a conventional three-electrode configuration consisting of platinum working and auxiliary electrodes and a Ag/AgCl reference electrode containing aqueous 3 M KCl. The solvent used in all experiments was CH_2Cl_2 (Merck HPLC grade), which was deoxygenated before use. The supporting electrolyte was 0.1 M tetrabutylammonium hexafluorophosphate. $E_{1/2}$ values were determined as $1/2(E_a + E_c)$, where E_a and E_c are the anodic and cathodic peak potentials, respectively. Magnetic measurements were done on a polycrystalline sample with a commercial SQUID susceptometer (Quantum Design MPMS-XL-5) in the temperature range 2−300 K with an applied magnetic field of 0.05 T. The sample susceptibility was corrected for the sample holder contribution, previously measured in the same conditions, and for the diamagnetic contribution of the constituent atoms (Pascal's tables).

Mössbauer Spectroscopy. Mössbauer spectra were collected in the 4−295 K temperature range, in transmission mode, using a conventional constant-acceleration spectrometer and a 25 mCi ^{57}Co source in a Rh matrix. The velocity scale was calibrated using α-Fe foil. Isomer shifts (ISs) are given relative to metallic α-Fe at 295 K. The disk-shaped absorbers were obtained by gently packing the samples into a perspex holder. Low-temperature spectra were collected using a liquid-helium JANIS bath cryostat with the sample in He exchange gas or, for measurements at 4.1 K, immersed in liquid He. The spectra were fitted to Lorentzian lines using a nonlinear least-squares method.[16]

General Procedures. All reactions were carried out under a nitrogen atmosphere using standard Schlenck techniques. Cluster $Mo_3(FeCl)S_4(dmpe)_3Cl_3$ (**1**) was prepared according to literature methods.[9] The remaining reactants were obtained from commercial sources and used as received. Solvents for synthesis were dried and degassed by standard methods before use.

$Mo_3(FeCN)S_4(dmpe)_3Cl_3$ (2). Compound **1** (15 mg, 0.014 mmol) was dissolved in 6 mL of CH_2Cl_2, and $(n\text{-}Bu_4N)CN$ (38 mg, 0.141 mmol) dissolved in CH_2Cl_2 (2 mL) was added under argon atmosphere. The reaction mixture was stirred at room temperature for 3 h observing a progressive color change from brown to green. The reaction mixture was taken to dryness, and the resultant viscous green solid was washed with water, isopropanol, and diethyl ether (12 mg, 81%). Found: C, 21.51; H, 4.76; N, 1.28%. $Mo_3FeS_4C_{19}H_{48}NCl_3P_6$ requires C, 21.64; H, 4.59; N, 1.33%. IR (KBr, cm^{-1}): 2109 (ν_{CN}). ESI-MS(+) *m/z*: 1054.7 $[M]^+$.

$Mo_3(FeN_3)S_4(dmpe)_3Cl_3$ (3). This compound was prepared following the method described for **2** by using **1** (50 mg, 0.047 mmol) and $(n\text{-}Bu_4N)N_3$ (134 mg, 0.47 mmol). In this case, reaction proceeded without a color change (45 mg, 90%). Found: C, 19.98; H, 4.61; N, 4.05%. $Mo_3FeS_4C_{18}H_{48}N_3Cl_3P_6$ requires C, 20.19; H, 4.52; N, 3.93%. IR (KBr, cm^{-1}): 2053 (ν_{N3}). ESI-MS(+) *m/z*: 1070.7 $[M]^+$.

$Mo_3(FeSPh)S_4(dmpe)_3Cl_3$ (4). Compound **1** (15 mg, 0.014 mmol) was dissolved in 6 mL of CH_2Cl_2, and $(n\text{-}Bu_4N)SPh$ (50 mg, 0.141 mmol) dissolved in CH_3OH (1.5 mL) was added under argon atmosphere. After 5 min, the reaction mixture was taken to dryness, and the resultant viscous dark solid was washed with water, isopropanol, and diethyl ether to obtain a brown-yellow solid (15 mg, 92%). Found: C, 25.29; H, 4.82%. $Mo_3FeS_5C_{24}H_{53}Cl_3P_6$ requires C, 25.33; H, 4.70%. ESI-MS(+) *m/z*: 1137.7 $[M]^+$.

Isolation of a 55/45 Mixture of $Mo_3(FeCl)S_4(dmpe)_3Cl_3$ (1) and $[Mo_3(FeCl)S_4(dmpe)_3Cl_3]PF_6$ ([1]PF_6). To a CH_2Cl_2 solution (125 mL) of complex **1** (980 mg, 0.92 mmol) was added a CH_2Cl_2:CH_3OH (12:1) solution (75 mL) of $NOBF_4$ (130 mg, 1.11 mmol) under argon

Table 1. Crystallographic Data for $[Mo_3(FeCl)S_4(dmpe)_3Cl_3]BF_4{\cdot}Et_2O$ ($[\mathbf{1}]BF_4{\cdot}Et_2O$), $Mo_3(FeCN)S_4(dmpe)_3Cl_3$ (**2**), and $Mo_3(FeN_3)S_4(dmpe)_3Cl_3{\cdot}CH_2Cl_2$ ($\mathbf{3}{\cdot}CH_2Cl_2$)

compd	$[\mathbf{1}]BF_4{\cdot}Et_2O$	**2**	$\mathbf{3}{\cdot}CH_2Cl_2$
empirical formula	$C_{22}H_{58}BCl_4F_4FeMo_3OP_6S_4$	$C_{19}H_{48}Cl_3FeMo_3NP_6S_4$	$C_{19}H_{50}Cl_5FeMo_3N_3P_6S_4$
formula weight	1225.02	1054.66	1155.60
crystal system	monoclinic	hexagonal	hexagonal
a (Å)	12.612(4)	15.534(3)	15.8488(5)
b (Å)	22.213(7)		
c (Å)	16.358(5)	29.177(11)	28.9890(19)
α (°)			
β (°)	90.629(8)		
γ (°)			
V (Å^3)	4583(2) Å^3	6097(3)	6306.0(5)
T (K)	293(2)	293(2)	293(2)
space group	$P2(1)/n$	$R3c$	$R3c$
Z	4	6	6
μ(Mo Kα) (mm^{-1})	1.774	1.907	1.977
reflections collected	21213	12555	16050
ϕ range for data collection	1.55−25.00	2.06−27.50	2.04−30.55
unique reflections/R_{int}	7918 [R(int) = 0.1318]	3111 [R(int) = 0.0769]	4052 [R(int) = 0.0741]
goodness-of-fit on F^2	0.990	1.093	1.029
$R1^a/wR2^b$	$R1$ = 0.0726, $wR2$ = 0.1542	$R1$ = 0.0477, $wR2$ = 0.1173	$R1$ = 0.0453, $wR2$ = 0.0933
$R1^a/wR2^b$ (all data)	$R1$ = 0.1721, $wR2$ = 0.1928	$R1$ = 0.0591, $wR2$ = 0.1254	$R1$ = 0.0952, $wR2$ = 0.1119
residual ρ (e A^{-3})	1.180 and −1.027	1.347 and −1.304	0.720 and −1.083

$^a R1 = \sum||F_0| - |F_c||/\sum F_0$. $^b wR2 = \{\sum[w(F_0^2 - F_c^2)^2]/\sum[w(F_0^2)^2]\}^{1/2}$.

atmosphere. The reaction mixture was stirred for 20 min at room temperature without any apparent color change. Layering diethylether to this solution yields the formation of a few single crystals of $[\mathbf{1}]BF_4{\cdot}Et_2O$, which were separated manually, along with other products. ESI mass analysis reveals the formation of $[Mo_3S_4(dmpe)_3Cl_3]^+$ corresponding to iron decoordination (signal at m/z 973) along with other cubane-type clusters. For example, the $[Mo_3(FeNO)S_4(dmpe)_3Cl_3]^+$ cation (signal at m/z 1058) coexists with $[Mo_3(FeCl)S_4(dmpe)_3Cl_3]^+$ (signal at m/z 1063), although their charge state in solution (neutral or singly charged) could not be determined by ESI-MS. Attempts to obtain $\mathbf{1}^+$ in a pure form were conducted as follows: after evaporation of the solvent, the resulting brown precipitate was redissolved in CH_2Cl_2 and adsorbed onto the silica gel column. Purification by column chromatography affords two different fractions; a first major green fraction is eluted with a KPF_6 solution in CH_3CN (1 mg/mL), which contains the trinuclear $[Mo_3S_4(dmpe)_3Cl_3]^+$ complex and in minor amounts the cluster resultant of the Cl to NO replacement at the Fe site. A second fraction is eluted with CH_3OH/KPF_6 mixtures (1 mg/mL), which contains a mixture of **1** and $[\mathbf{1}]PF_6$. The second fraction was taken to dryness redissolved in CH_2Cl_2 and filtered to remove the insoluble KPF_6 inorganic salt. After CH_2Cl_2 evaporation to a brown precipitate of **1** and $[\mathbf{1}]PF_6$ was afforded. Repeated synthesis by using different **1** to $NOBF_4$ ratios and temperature conditions invariably lead to this mixture of products. All attempts to obtain $[\mathbf{1}]PF_6$ in pure form have failed. For the spectroscopic studies shownd below, we use the same sample, which contains ca. 55/45 of $\mathbf{1}/[\mathbf{1}]PF_6$ as evidenced by elemental analysis, susceptibility magnetic measurements, and ^{57}Fe Mössbauer.

X-ray Crystallographic Study. Single-crystals of compounds **2** and **3** were obtained layering diethyl ether to dichloromethane solutions of **2** and **3**. Single crystals of compound $[\mathbf{1}]BF_4$ were obtained directly from the reaction mixture between **1** and $NOBF_4$ (see the Experimental Section) by slow diffusion of ether. The crystals were air stable and were mounted on the tip of a glass fiber with the use of epoxy cement. X-ray diffraction experiments were carried out on a Bruker SMART CCD diffractometer using Mo Kα radiation (λ = 0.71073 Å) at room temperature. Data were collected with a frame width of 0.3° in ω at a crystal to detector distance of 4 cm. The diffraction frames were integrated using the SAINT package and corrected for absorption with SADABS.[17] The structures were solved by direct methods and refined by the full-matrix method based on F^2 using the SHELXTL software package.[18] The crystal parameters and basic information relating data collection and structure refinement for compounds $[Mo_3(FeCl)S_4(dmpe)_3Cl_3]BF_4{\cdot}Et_2O$ ($[\mathbf{1}]BF_4{\cdot}Et_2O$), $Mo_3(FeCN)S_4(dmpe)_3Cl_3$ (**2**), and $Mo_3(FeN_3)S_4(dmpe)_3Cl_3{\cdot}CH_2Cl_2$ ($\mathbf{3}{\cdot}CH_2Cl_2$) are summarized in Table 1.

Compound $[\mathbf{1}]BF_4{\cdot}Et_2O$ crystallizes in the monoclinic $P2(1)/n$ space group, whereas **2** and $\mathbf{3}{\cdot}CH_2Cl_2$ are isostructural and crystallize in the space group $R3c$ with Flack absolute structure parameters being refined as 0.44(5) and 0.04(5), respectively. For compounds $[\mathbf{1}]BF_4{\cdot}Et_2O$, **2**, and $\mathbf{3}{\cdot}CH_2Cl_2$, the nonhydrogen atoms of the cluster and the counteranion were refined anisotropically, while the positions of all hydrogen atoms in the diphosphane ligands were generated geometrically, assigned isotropic thermal parameters, and allowed to ride on their respective parent carbon atoms. For compound $\mathbf{3}{\cdot}CH_2Cl_2$, the nitrogen atom [N(1)] attached to the Fe atom lies on a special position, while N(2) and N(3) are in general positions, and their occupancies were adjusted to be compatible with one N_3^- group per Mo_3FeS_4 cluster. Diethylether and dichloromethane molecules of crystallization were found in the last Fourier map in compounds $[\mathbf{1}]BF_4{\cdot}Et_2O$ and $\mathbf{3}{\cdot}CH_2Cl_2$, which were refined isotropically under rigid conditions.

Computational Methods. All calculations were carried out using the G09 program.[19] All species studied were calculated using the geometry of the X-ray structure using DFT calculations, in particular the B3LYP approximation,[20] combined with the Stuttgart−Desden pseudopotentials for Mo and Fe and the 6-31G(d) basis set for the remaining atoms. Unrestricted calculations were carried out, but the $\langle S^2\rangle$ ($\langle S^2\rangle$ = the expectation value of the total spin operator) values shown severe deviations from the theoretical values (2.44 and 2.28 for triplet state and 1.73 for a doublet state), and the restricted open formalism was employed instead to ensure the calculation of pure electronic states.

■ RESULTS AND DISCUSSION

Substitutional Lability at the Fe Site and Redox Series in Mo_3FeS_4 Clusters. Heterobimetallic Mo_3FeS_4 clusters described in this work are accessible by ligand-substitution

Scheme 2

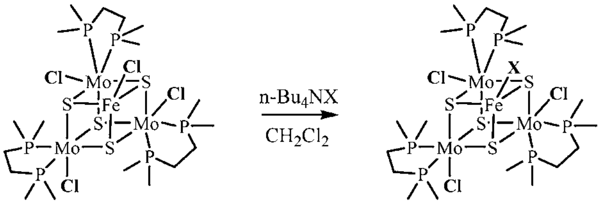

X = CN (**2**); X = N$_3$ (**3**); X = SPh (**4**)

reactions of $Mo_3(FeCl)S_4(dmpe)_3Cl_3$ (**1**) in dichloromethane (see Scheme 2 where numbering of compounds investigated in this work is also depicted).

Treatment of **1** with 10 equiv of tetrabutylammonium salts *n*-Bu_4NX (X = CN^-, N_3^-, SPh^-) affords $Mo_3(FeCN)S_4(dmpe)_3Cl_3$ (**2**), $Mo_3(FeN_3)S_4(dmpe)_3Cl_3$ (**3**), and $Mo_3(FeSPh)S_4(dmpe)_3Cl_3$ (**4**), respectively. Reaction yields are quantitative so this protocol represents a general synthetic entry to $Mo_3FeS_4^{4+}$ clusters selectively substituted at the Fe site. This substitution reaction follows from earlier demonstrations of the versatility of cluster **1** to enter selective ligand substitution reactions at the Fe and Mo sites with sodium salts such as NaSPh.[9] Remarkably, ligand substitution at the Mo sites does not occur even using an excess of *n*-Bu_4NX salts, the use of alkali NaX salts being necessary to access substitutional lability of the Mo−Cl bonds. This increased reactivity of the Fe versus Mo sites is also observed for the closely related $(Et_4N)[MoCl(FeCl)_3S_4(dmpe)]$ cluster in which the coordination environment at both Mo and Fe sites is identical to that found in **1**.[21] Clusters **2** and **3** exhibit characteristic $\nu(CN)$ and $\nu(N_3)$ stretching frequencies in their IR spectra at 2109 and 2053 cm^{-1}, respectively. The crystal structures of compounds **2** and **3** were determined by X-ray crystal structure analysis, and ORTEP representations are illustrated in Figure 1.

Like compounds **1** and **4**,[9] the cluster core of compounds **2** and **3** consists of a slightly distorted tetrahedral arrangement of one iron and three molybdenum atoms. Each tetrahedral face is capped by a μ_3-coordinated sulfur atom, thus generating a cubane-like structure. Each molybdenum atom presents a pseudooctahedral coordination environment, with two out of three external positions being occupied by the phosphorus atoms of the dmpe ligand. The third position is occupied by a chlorine atom. In **2** and **3**, the iron atom presents a pseudotetrahedral environment defined by three S atoms and a CN group that appears perfectly linear imposed by crystal symmetry (for **2**) and a N_3 group almost lineal (N−N−N, 171°) that appears bent (Fe−N−N, 128.5°). As far as the effect on Cl^-, CN^-, N_3^-, or SPh^- ligation at the Fe site is concerned, the structures of **1**−**4**, which contain the $Mo_3FeS_4^{4+}$ core, are subtly distinguishable from one another (see Table 2), in terms of core Mo−Fe and Fe−S dimensions. Upon CN ligation, a shortening of the Mo−Fe bond distance of ca. 0.025 Å is seen, which is also manifested in a shortening of Fe−S bonds, overall resulting in a slight $Mo_3FeS_4^{4+}$ core contraction. The remaining Mo−Mo and Mo−S bond distances remain largely unchanged.

Positive ESI mass spectrometry proved to be a very useful technique for characterization purposes of the neutral cubane-type Mo_3MS_4 (M = Co, Ni) clusters bearing diphosphane ligands[22] and also for Mo_3FeS_4.[9] Like compounds **1** and **4**, the ESI mass spectrum of compounds **2** and **3** gives abundant signals due to the $\mathbf{2}^+$ and $\mathbf{3}^+$ molecular ions, accompanied by minor peaks corresponding to sodium adducts and X^- losses (where X stands for Cl^-, CN^-, N_3^-, or SPh^-) to yield species of general formula $[M + Na]^+$, $[M - FeX]^+$, and $[M - X]^+$, respectively. For all compounds **1**−**4**, the one electron detachment mechanism is clearly favored under ESI conditions to yield $\mathbf{1}^+$−$\mathbf{4}^+$, and this feature anticipates oxidation redox chemistry for these Mo_3FeS_4 complexes most likely associated to the $\mathbf{1}$−$\mathbf{4}/\mathbf{1}^+$−$\mathbf{4}^+$ redox couples. In general, the redox versatility in Mo_3FeS_4 clusters bearing aqua, NH_3, and hydrotris(pyrazolyl)borate is well-documented as judged by cyclic voltammetry analysis and spectroscopic techniques;[10−12] however, isolation in substance of members of the electron transfer Mo_3FeS_4 series still remains unknown. For example, cyclic voltammetry experiments of compound $Mo_3(FeCl)S_4Tp_3$ (Tp = hydrotris(pyrazolyl)borate),[12] show monoelectronic reduction and oxidation reversible waves at $E_{1/2} = -1.40$ and one 0.52 V (vs SCE), respectively. Two irreversible one-electron oxidation processes $E_{pc} = 1.54$ and 1.66 V (vs SCE) are also observed. Oxidation and reduction waves, except that observed at $E_{pc} = 1.66$ V, were assigned to monoelectronic redox changes confined to the Mo_3 subunit. Identical redox behavior in its cyclic voltammogram, in terms of confinement in the Mo_3 units, has been reported for the aqua $[Mo_3(FeH_2O)$-

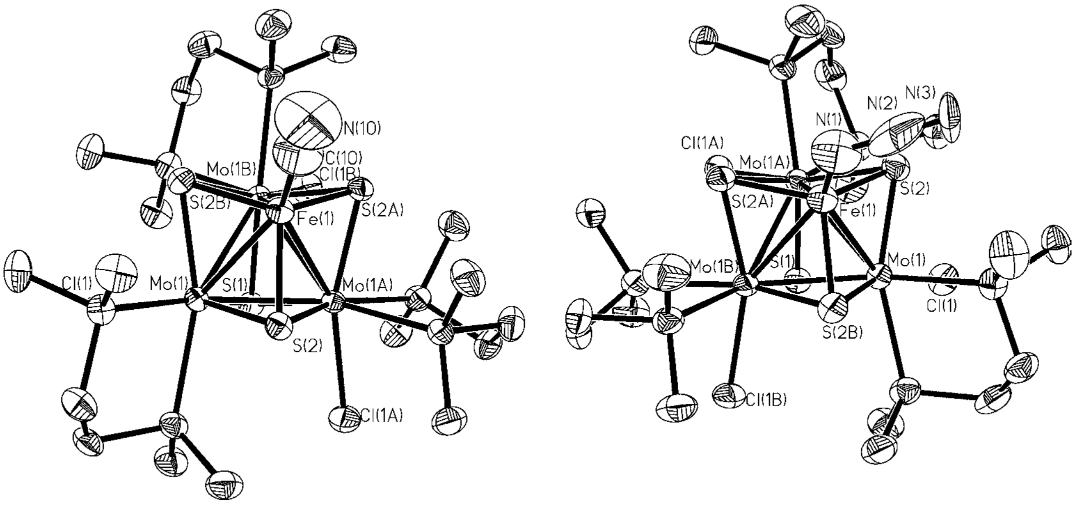

Figure 1. ORTEP representation (50% probability ellipsoids) of compounds **2** and **3**.

Table 2. Selected Averaged Bond Distances (Å) for Compounds $Mo_3S_4(FeCl)(dmpe)_3Cl_3 \cdot CH_2Cl_2$ ($1 \cdot CH_2Cl_2$), $Mo_3(FeCN)S_4(dmpe)_3Cl_3$ (2), $Mo_3(FeN_3)S_4(dmpe)_3Cl_3 \cdot CH_2Cl_2$ ($3 \cdot CH_2Cl_2$), $Mo_3(FeSPh)S_4(dmpe)_3Cl_3$ (4), and $[Mo_3(FeCl)S_4(dmpe)_3Cl_3]BF_4 \cdot Et_2O$ ($[1]BF_4 \cdot Et_2O$)[a]

distance (Å)	Mo−Mo	Mo−Fe	Mo−Cl	Fe−(μ_3-S)	Fe−L	ref
$Mo_3(FeCl)S_4(dmpe)_3Cl_3$ (1)	2.8111(8)	2.7358(12)	2.5272(14)	2.2483(15)	2.211(3)	9
$Mo_3(FeCN)S_4(dmpe)_3Cl_3$ (2)	2.8019(11)	2.7077(15)	2.522(2)	2.232(2)	2.09(2)	this work
$Mo_3S_4(FeN_3)(dmpe)_3Cl_3$ (3)	2.8131(9)	2.7333(14)	2.527(2)	2.249(2)	1.950(13)	this work
$Mo_3(FeSPh)S_4(dmpe)_3Cl_3$(4)	2.804[9]	2.725[11]	2.526[14]	2.241[11]	2.270(8)	9
$[Mo_3(FeCl)S_4(dmpe)_3Cl_3]BF_4$ ($[1]BF_4$)	2.7918(17)	2.759(2)	2.489(3)	2.240(4)	2.209(5)	this work
	2.8019(16)	2.774(2)	2.477(4)	2.263(4)		
	2.8133(16)	2.802(2)	2.466(4)	2.279(4)		

[a] Standard deviations are given in parentheses, and standard deviations for averaged values are given in square brackets.

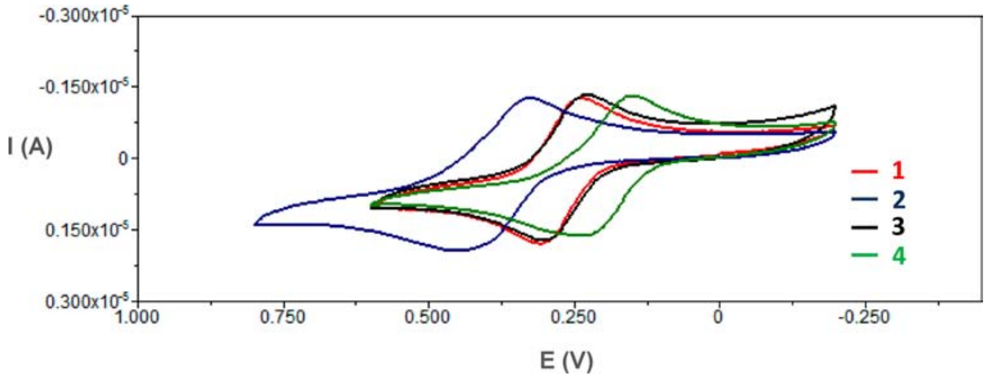

Figure 2. Cyclic voltammograms of compounds 1−4 recorded in CH_2Cl_2 at 100 mV/s.

Table 3. Redox Potentials[a] for the Series of Cubane-Type $Mo_3(FeX)S_4(dmpe)_3Cl_3$ Where X^- = Cl^-, CN^-, N_3^-, and SPh^-

	oxidation $E_{1/2}$ (ΔE^c)	
compd	mV	V
$Mo_3(FeCl)S_4(dmpe)_3Cl_3$ (1)	0.26 (76)	1.06 (160)
$Mo_3(FeCN)S_4(dmpe)_3Cl_3$ (2)	0.38 (114)	1.16[b]
$Mo_3(FeN_3)S_4(dmpe)_3Cl_3$ (3)	0.25 (81)	1.01 (143)
$Mo_3(FeSPh)S_4(dmpe)_3Cl_3$ (4)	0.16 (99)	1.03 (241)

[a] $E_{1/2}$ (ferrocene/ferrocene$^+$) = 0.44 V (ΔE = 66 mV). [b] Potentials measured at 100 mV s^{-1}. [c] $\Delta E = |E_a - E_c|$ measured at a scan rate of 100 mV s^{-1}.

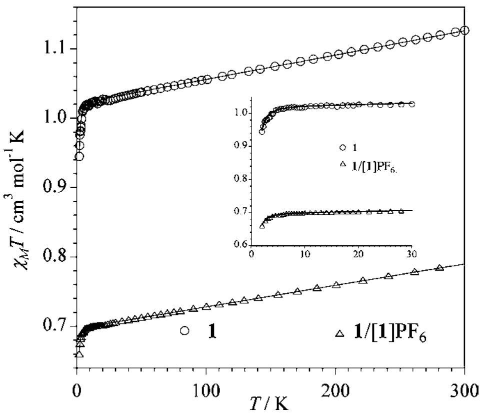

Figure 3. Thermal dependence of the $\chi_M T$ product for 1 and the 1/[1]PF_6 mixture. The solid line is the theoretical curve based on eqs 1−3; see the text. The inset shows the low-temperature region.

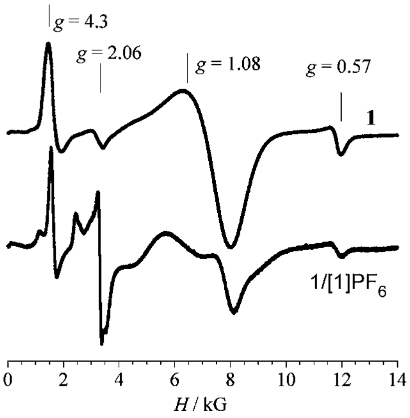

Figure 4. X-band EPR spectra of polycrystalline samples of 1 and the 1/[1]PF_6 mixture at 4.5 K.

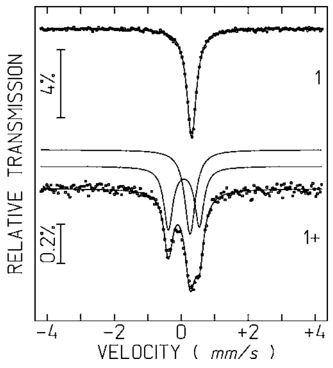

Figure 5. Mössbauer spectra taken at room temperature of complexes 1 and the 1/[1]PF_6 mixture.

Table 4. Estimated Parameters[a] from the ^{57}Fe Mössbauer Spectra Taken at Different Temperatures *T*

compd	*T* (K)	IS	QS	*I* (%)
$Mo_3(FeCl)S_4(dmpe)_3Cl_3$ (**1**)	295	0.42	0.05	100
	4	0.52	0.11	100
$Mo_3(FeCN)S_4(dmpe)_3Cl_3$ (**2**)	295	0.30	0.90	100
$Mo_3(FeN_3)S_4(dmpe)_3Cl_3$ (**3**)	295	0.39	0.27	100
$Mo_3(FeSPh)S_4(dmpe)_3Cl_3$ (**4**)	295	0.35	0.49	100
$[Mo_3(FeCl)S_4(dmpe)_3Cl_3]PF_6$, ([**1**]$PF_6$) impurity (compound **1**)	295	0.14	0.60	45
	4	0.42	0.05	55
		0.25	0.70	45
		0.52	0.11	55

[a] IS, isomer shift relative to metallic α-Fe at room temperature (mm/s); QS, quadrupole splitting (mm/s); *I*, relative area (%). Estimated standard deviations are <2% for I and <0.02 mm/s for the other parameters.

Scheme 3. Representation of Molecular Orbital Diagram for Clusters **1** and **1**$^+$. Orbital energies in a.u.

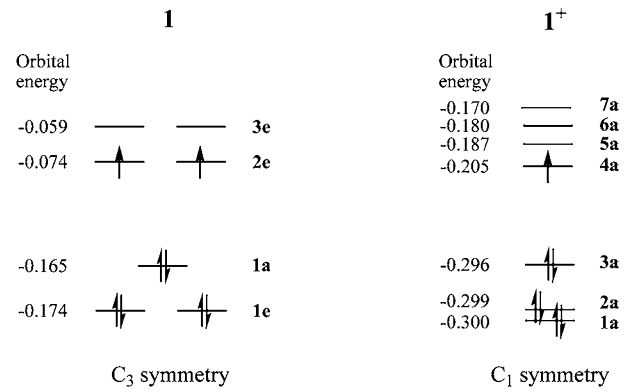

$S_4(H_2O)_9]^{4+}$ cluster where a formal oxidation state of $Mo^{IV}Mo^{III}{}_2Fe^{II}$ has been proposed for the $Mo_3FeS_4{}^{4+}$ core.[10] In the present work, we investigate the accessibility of redox states in **1**−**4** by cyclic voltammetry in CH_2Cl_2 solution versus Ag/AgCl. Potentials reported are referenced to $E_{1/2}$ (ferrocene/ferrocene$^+$) = 0.44 V. Figure 2 shows cyclic voltammograms for compounds **1**−**4** in the 0.25−0.85 V range.

An oxidation wave is observed for the four compounds in the 0.17−0.39 V range that displayed features of chemical quasireversibility on the basis of constant i_{pa}/i_{pc} ratio and the peak-to-peak separation in the 76−114 mV range measured at a scan rate of 100 mV s^{-1}. Redox potentials are collected in Table 3 and represent the first comparative effect of X ligation at the Fe site on redox potentials. These results establish the oxidizability order when L ligands are attached at the Fe site from L = SPh^- > Cl^- = $N_3{}^-$ > CN^- at parity of molybdenum terminal ligands. These changes are substantial (encompassing 160 mV) and in particular for the CN-substituted complex **2**. Similarly, cyanide ligation at the Fe sites has been recently reported in Fe_4S_4 and $MoFe_3S_4$ clusters, revealing a significant efficiency for the stabilization of lower oxidation states.[23] In contrast, the first reduction potential of $[Mo_3(CuX)S_4(dmpe)_3Cl_3]^+$ cluster (X^- = Cl^-, CN^-, $CN^-\cdots Mo(CO)_5$, at parity of ligands at molybdenum sites) does not show any significant change upon replacement of the X ligand attached to copper.[24]

We find that iron incorporation into the $[Mo_3S_4(dmpe)_3Cl_3]^+$ cation produces heterobimetallic complexes, which are easier to oxidize and more difficult to reduce than their trimetallic cluster precursors, as previously reported for the iron insertion into the $[Mo_3S_4(H_2O)_9]^{4+}$ aquo ion. In fact, complexes **1**−**4** do not show any reduction wave within the dichloromethane/(*n*-$Bu_4N)PF_6$ solvent window. For **1**, **3**, and **4**, quasi-reversible oxidation waves are also observed at ca. $E_{1/2}$ = 1.0 V. The peak currents are all substantially larger than the primary one electron step, and most likely, this involves a two electron step. For complex **2**, an irreversible oxidation process is also observed, that we tentatively associate with iron decoordination from the cubane-like Mo_3FeS_4 cluster core.

As is evident from the voltammograms in Figure 2 and also from ESI mass spectra, the **1**−**4** family sustains a two-member redox series most likely associated with the $Mo_3FeS_4{}^{4+,5+}$ redox couples. On the basis of the observed potentials, we prompt to investigate the possibility of chemical oxidation to the $[Mo_3(FeX)S_4Cl_3(dmpe)_3]^+$ cluster. We face the isolation of this new $Mo_3FeS_4{}^{5+}$ redox state by using a number of oxidants. The use of different oxidant such as I_2, TCNQ, and $PhICl_2$ was unsuccessful, leading in most cases to unwanted X to I^- replacement accompanied by **1**−**4** cluster dismantling to yield the trinuclear $[Mo_3S_4(dmpe)_3Cl_3]^+$ precursor. While for the derivatives **2**−**4** with X = CN^-, $N_3{}^-$, and SPh^-, all attempts to isolate **2**$^+$−**4**$^+$ were unsuccessful, we succeed at isolating single crystals of the oxidized cubane-type $[Mo_3(FeCl)S_4(dmpe)_3Cl_3]BF_4$ ([**1**]BF_4) cluster by reaction of **1** with $NOBF_4$ followed by slow diffusion of diethylether into the resulting mixture. Attempts to obtain the **1**$^+$ cation in pure form were carried out by silica gel chromatography. Compound **1**$^+$ was eluted with methanol and KPF_6 mixtures and invariably eluted with compound **1**. After repeated synthesis, elemental

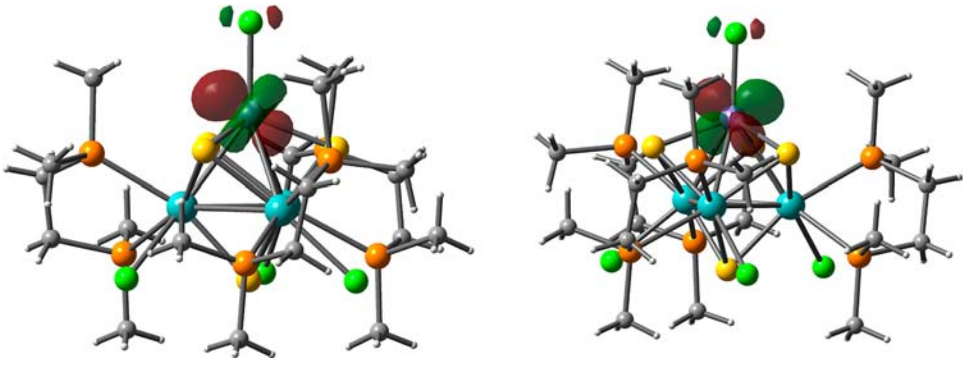

Figure 6. Isocontour plots for the degenerate SOMOs (orbitals 2e) of cluster **1**.

analysis of bulk samples of [**1**]PF_6 was not satisfactory and suggests the presence of impurities of compound **1** as judged by susceptibility measurements and ^{57}Fe Mössbauer spectroscopy (see purification details in the Experimental Section) so that further spectroscopic investigations were carried out on a sample containing [**1**]PF_6 and **1** in a ca. 45:55 ratio.

Experimental Determination of Ground States and Oxidation States in $Mo_3FeS_4^{4+,5+}$. Harris et al.[25] have proposed a theoretical scheme for these $Mo_3M'S_4$ (M = Co, Ni, Pd, Sn) clusters with 14−16 metal electrons, where two or four electrons partially or fully occupy the HOMO orbital with an "e" symmetry. Support to this MO scheme is given by the X-ray analysis and magnetic properties previously reported for the series of Mo_3CoQ_4 clusters (Q = S, Se) bearing diphosphane ligands.[8,26] Aimed to validate whether this model is also applicable to the homologous Mo_3FeS_4 series, a detailed analysis of the intracluster bond distances, magnetic properties, and Mössbauer spectroscopy of compounds **1** and $\mathbf{1}^+$ is carried out.

Intracluster Bond Distance Analysis. The crystal structure analysis of [**1**]BF_4 revealed identical molecular organization, in terms of intracluster metal and sulfur atoms disposition, to that found in **1**. Comparison of mean bond lengths of **1** and $\mathbf{1}^+$ (Table 2) reveals an increase of the Mo−Fe (ca. 0.04 Å) bond upon oxidation also manifested in the elongation of Fe−S (ca. 0.01 Å) distances, while Mo−Mo bond distances remain essentially unchanged. This experimental observation suggests that Mo_3FeS_4 cluster core dismantling via Fe decoordination is more prone for $Mo_3FeS_4^{5+}$. Mo−Cl bond distances are elongated (ca. 0.05) on going from $\mathbf{1}^+$ to **1**, suggesting that the removed electron occupies a molecular orbital with bonding and nonbonding character with respect to the Mo−Fe and Mo−Mo bonds, respectively, and antibonding with respect to the Mo−Cl bonds. We also observed a noticeable distortion of the cluster core from its C_3 symmetry upon oxidation of **1** to afford $\mathbf{1}^+$ that results in three significantly different Mo−Mo and Mo−Fe bond lengths. Such distortion could be attributed to a Jahn−Teller distortion considering the degeneration of the doubly occupied HOMO orbital in **1**.

Magnetic Properties. The magnetic properties for **1**−**4** and the **1**/[**1**]PF_6 mixture have been studied in the 2.0−300 K temperature range. At room temperature, the $\chi_M T$ value for **1**−**4** is comparable ca. 1.15 cm^3 mol^{-1} K and agrees with a spin triplet ($S = 1$) for the **1**−**4** series (Figure S1 in the Supporting Information). For the sake of comparison between the $Mo_3FeS_4^{4+,5+}$ redox couple, the molar magnetic susceptibility and EPR measurements are described in detail below. Figure 3 shows the thermal dependence of the $\chi_M T$ product for **1** and the **1**/[**1**]PF_6 mixture (χ_M being the molar magnetic susceptibility).

At room temperature, the $\chi_M T$ value for **1** is 1.15 cm^3 mol^{-1} K. It decreases linearly with T until 1.02 at 7 K. Below this temperature, it decreases more sharply 0.94 at 2 K. This behavior is as expected for a spin triplet ($S = 1$) with zero-field splitting, D. In fact, the experimental susceptibility data can be perfectly simulated by using eq 1 with $g_{\|} = g_{\perp} = g_{S=1}$ and adding a temperature-independent paramagnetism term (χ_{TIP}). The best-fit parameters are as follows: $g_{S=1} = 2.02(1)$, $D = 1.5(1)$ cm^{-1}, and $\chi_{TIP} = 350(5) \times 10^{-6}$ cm^3 mol^{-1}.

$$\chi_{\|} = \frac{2N\beta^2 {g_{\|}}^2}{kT} \frac{\exp(-D/kT)}{1 + 2\exp(-D/kT)} \tag{1a}$$

$$\chi_{\perp} = \frac{2N\beta^2 {g_{\perp}}^2}{D} \frac{1 - \exp(-D/kT)}{1 + 2\exp(-D/kT)} \tag{1b}$$

$$\chi_{S=1} = \frac{\chi_{\|} + 2\chi_{\perp}}{3} + \chi_{TIP} \tag{1c}$$

Similar results were obtained for **2**−**4**: $g = 2.05(1)$, $D = 3.60(1)$ cm^{-1}, and $\chi_{TIP} = 400(6) \times 10^{-6}$ cm^3 mol^{-1} (for **2**); $g = 2.03(1)$, $D = 3.10(1)$ cm^{-1}, and $\chi_{TIP} = 450(7) \times 10^{-6}$ cm^3 mol^{-1} (for **3**); and $g = 2.03(1)$, $D = 1.70(1)$ cm^{-1}, and $\chi_{TIP} = 420(6) \times 10^{-6}$ cm^3 mol^{-1} (for **4**). The **1**/[**1**]PF_6 mixture exhibits a similar $\chi_M T$ versus T plot regarding that observed for **1**, but the $\chi_M T$ values are smaller. This is expected for a mixture of **1** and [**1**]PF_6 with spin values of $S = 1$ and $S = 1/2$, respectively. To reproduce theoretically the experimental susceptibility data, eq 2 was used (a χ_{TIP} term was also added), where $\chi_{S=1}$ and $\chi_{S=1/2}$ are calculated by means eqs 1 and 3, respectively. The ρ parameter takes into account the molar fraction of **1** in the mixture. In the fitting process, the corresponding magnetic parameters of **1** ($g_{S=1} = 2.02$ and $D = 1.5$ cm^{-1}) were kept constant. Moreover, the $g_{S=1/2}$ and ρ parameters are totally correlated, as one can see from eqs 2 and 3 ($\rho\chi_{S=1/2} = [N\beta^2/4kT]\rho g^2_{S=1/2}$). So, we also fixed $g_{S=1/2} = 2.06$ (the observed value from electron paramagnetic resonance spectra, see below) in the fitting process. The best-fit parameters through eq 2 are as follows: $\rho = 0.48(1)$ and $\chi_{TIP} = 310(5) \times 10^{-6}$ cm^3 mol^{-1}.

$$\chi_M = (1 - \rho)\chi_{S=1/2} + \rho\chi_{S=1} \tag{2}$$

$$\chi_{S=1/2} = \frac{N\beta^2 {g_{S=1/2}}^2}{4kT} \tag{3}$$

The value of ρ (ca. 0.48) is close to that observed from elemental analysis and ^{57}Fe Mössbauer spectroscopy ($\rho \approx 0.45$). The experimental susceptibility data were carefully corrected for the diamagnetism of both the constituent atoms and the sample holder, as indicated in the Experimental Section. So, the temperature-independent paramagnetism observed (χ_{TIP}) must be attributed specially to the molybdenum atoms. These results agree with the occurrence of a triplet spin ground state, $S = 1$, for **1**, and they support the model proposed by Harris et al.[25] for this kind of cluster with 14 metal electrons. From this theoretical model, the oxidation of **1** would produce a cluster with 13 metal electrons, giving thus a ground spin doublet, as suggested from the magnetic susceptibility analysis of the **1**/[**1**]PF_6 mixture.

The ground spin state of **1**−**3** and [**1**]PF_6 is further confirmed by the X-band electron paramagnetic resonance (EPR) spectra. Figure 4 shows the spectra of compounds **1** and [**1**]PF_6 at 4.5 K. Figures S2 and S3 in the Supporting Information display EPR spectra at different temperatures. That of **1** provides clear evidence of the presence of a ground spin triplet, $S = 1$, with a zero-field splitting, $D > h\nu$,[27] ($h\nu \approx 9.5$ GHz ≈ 0.3 cm^{-1}). Similar spectra were observed for **2** and **3** (Figure S4 in the Supporting Information). Compound **4** gives poor quality spectra from which reliable g values cannot be determined. The spectrum of the **1**/[**1**]PF_6 mixture is that of **1** except for an additional anisotropic signal centered at $g = 2.06$, a feature that is consistent with a ground spin doublet, $S = 1/2$, for [**1**]PF_6.

^{57}Fe Mössbauer Spectroscopy. Selected ^{57}Fe Mössbauer spectra taken at 295 K of compounds **1**−**4** and the **1**/[**1**]PF_6

mixture are shown in Figure 5. The spectra obtained at 4 K are very similar to those obtained at room temperature for the same compounds. Estimated ISs and quadrupole splittings (QS) are collected in Table 4 for the whole **1**−**4** series. Attempts to fit the Mössbauer spectra of compound **1** with a quadrupole doublet lead to vanishingly small QS, while QS values in the 0.27−0.90 (mm/s) range were estimated for **2**−**4**. Spectra with a single absorption peak as in **1** have been previously observed for $[Mo_3(FeH_2O)S_4(NH_3)_9]^{4+}$ in frozen solutions and $[Mo_3(FeH_2O)S_4(H_2O)_9](pts)_4{\cdot}7H_2O$.[28] The origin for such low QS values remains unknown given that the point symmetry at the Fe atom in compound **1** is not cubic. A very low QS value may be due to a particular ground state occupation of the Fe *d* orbitals in which the contributions to the electric field gradient cancel, as found for a few Fe *S* = 1 complexes.[29] The estimated IS for compound **1** is the same within experimental error as the reported value for the FeS_3Cl unit in the $[Fe_4S_4Cl_4]^{2-}$ delocalized cluster where iron has an average +2.5 oxidation state.[30] A linear dependence of experimental IS values and formal oxidation states of Fe in tetrahedral FeS_{4-n} $(SR)_n$ units has been reported.[31] However, this relationship may not give precise formal oxidation states for tetrahedral FeS_3L units with L = Cl^-, PR_3, etc. In fact, the IS for these units in Fe_4S_4, $MoFe_3S_4$, and VFe_3S_4 clusters depend on L, usually decreasing in the order L = $Cl^- > RS^- > PR_3$.[32] In the present case where FeS_3L units are incorporated in Mo_3FeS_4 clusters, a similar decrease of IS is observed when the Cl^- ligand is replaced by the thiolate SPh^-. The IS values are similar for Cl^- and N_3^- ligands (within experimental error). The lowest IS is observed for the CN^- ligand. We did not find any Mössbauer data in the literature for a FeS_3CN unit incorporated in cubane-type clusters. The significant decrease in IS measured for **2** relative to **1** may tentatively be explained by the π acceptor properties of the CN^- ligand.[29] The metal to ligand π donation into unfilled ligand π*-orbitals in compound **2** causes a lowering of the *d* electron density at the Fe atom and an increase in the *s* electron density at the Fe nuclei that results in lower IS values. For compounds **3** and **4**, where the π acceptor properties of the ligands are weaker, the decrease in IS is also smaller.

As explained above, compound $\mathbf{1}^+$ could not be obtained pure always containing a significant fraction of **1**. The corresponding spectrum shows a single peak due to **1** overlapping a doublet that may be attributed to $\mathbf{1}^+$. The IS of this doublet is 0.28 mm/s, lower than IS of **1**.

The strong increase in the QS of $\mathbf{1}^+$ relative to **1** (Table 4) may be explained by the noticeable distortion of the cluster core in **1** after oxidation to $\mathbf{1}^+$ that results in three significantly different Mo−Fe and Fe−S bond lengths (Table 2) as referred above. Because the ligands bonded to Fe in **1** and $\mathbf{1}^+$ are the same, this decrease in IS may only be attributed to the oxidation on going from $Mo_3FeS_4^{4+}$ to $Mo_3FeS_4^{5+}$. Hauser et al.[30] suggested that a decrease of 0.12 mm/s in the IS would approximately correspond to the removal of one delocalized electron from the VFe_3S_4 cluster and therefore a decrease of 1/3 electron per Fe atom. Still according to these authors, this deduction is consistent with the above referred linear dependence of experimental IS values and formal oxidation states of Fe in tetrahedral $FeS_{4-n}(SR)_n$ units. IS (1) − IS (1^+) = 0.28 mm/s (Table 4) would correspond to a 0.8 electrons decrease on the single Fe atom of the Mo_3FeS_4 cluster. Considering that differences may be expected between the electron density distribution in clusters containing 4 or 3 Fe atoms and those containing only 1, this quantitative prediction should be taken with caution. However, the decrease of 0.28 mm/s in the IS clearly shows a pronounced increase in the oxidation state of the Fe atom in $\mathbf{1}^+$ relative to **1**, strongly suggesting that oxidation is mainly centered at the Fe site and that the HOMO orbital in **1** has a significant contribution from Fe in agreement with the theoretical analysis below.

The panoply of experimental techniques presented above strongly suggests that the Fe oxidation state in **1** is close to +2. We therefore suggest that **1** and $\mathbf{1}^+$ are reasonably described as $[Mo_2^{III}Mo^{IV}Fe^{II}S_4]^{4+}$ and $\mathbf{1}^+$ as $[Mo_2^{III}Mo^{IV}Fe^{III}S_4]^{5+}$, in which case the redox event is largely confined to the Fe site and associated to a lesser extent to molybdenum and sulfur atoms. Recently, we have concluded that redox changes along the electron transfer $Mo_3CoS_4^{3+,4+,5+}$ series featuring diphosphane as ancillary ligands are mainly associated with the Co site.[8]

Theoretical Analysis of the Molecular Orbital Diagram in $Mo_3FeS_4^{4+,5+}$. The isolation of complexes **1** and $\mathbf{1}^+$ with 14 and 13 metal electrons, respectively, provides an ideal system to analyze the nature of the frontier orbitals of these complexes based on structural results. With the aim of rationalizing the experimental consequences of the different metal counting on the 14 and 13 electron species, namely, **1** and [**1**]PF_6, a DFT study on these structures have been carried out at the ROB3LYP level using X-ray geometries. A representation of molecular orbital (MO) diagram for clusters **1** and $\mathbf{1}^+$ is given in Scheme 3. Cluster **1** allocates two electrons in two degenerate orbitals, yielding a triplet ground state of C_3 symmetry. The calculated singlet state was found 38.8 kcal/mol less stable than the corresponding triplet state. Upon removal of one electron, cluster $\mathbf{1}^+$ suffers a small Jahn−Teller distortion, and the MOs are no longer degenerate, although they are essentially identical.

The **2e** orbitals (SOMOs) of cluster **1** are composed mainly (87% of atomic contribution to the MO; see the Supporting Information) by the Fe d_{zx} and d_{zy} atomic orbitals (see Figure 6) with a small contribution from the attached chlorine. On the other hand, the molecular orbitals **3e** (LUMO) are composed by a mixing of d atomic orbitals of Fe (18%) and Mo (52%) atoms, and they are very close in energy to the **2e** orbitals. Interestingly, **1a** and **1e** orbitals are also formed by a mixing of d orbitals of Fe and Mo atoms pointing out the delocalized nature of these MOs and the multiconfigurational character of the wave function, which cannot be handled by the unrestricted DFT formalism. From this MO picture, it can be deduced that the unpaired electrons of **1** and $\mathbf{1}^+$ clusters are located on the Fe atom, whitout participation of the ligand or the cluster unit.

■ CONCLUSIONS

We have further explored the chemistry of the Mo_3FeS_4 platform bearing diphosphane ligands, and through the combined use of cluster synthesis, extensive spectroscopic techniques, and DFT calculations, the following are the principal conclusions: (i) a general protocol to access $Mo_3(FeX)S_4(dmpe)_3Cl_3$ (X = Cl^-, CN^-, N_3^-, SPh^-) clusters selectively substituted at the Fe site is described based on the use of an excess of tetrabutylammonium salts *n*-Bu_4NX. (ii) Geometric parameters of the $Mo_3FeS_4^{4+}$ cluster core are identical for **1**, **3**, and **4**, whereas a shorthening of Mo−Fe and Fe−S bond distances (cluster contraction) is observed for the CN-substituted derivative. The relative stability toward $Mo_3FeS_4^{4+}$ to $Mo_3FeS_4^{5+}$ interconversion along the series **1**−**4** when L ligands are attached at the Fe site goes from L = SPh^-

> Cl^- = N_3^- > CN^- at parity of molybdenum terminal ligands. (iii) Ground states for **1** and **1**$^+$ are determined on the basis of a combination of experimental techniques that includes magnetic susceptibility, EPR measurements, and ^{57}Fe Mössbauer spectroscopy. (iv) The combined use of spectroscopic and theoretical descriptions of the **1**/**1**$^+$ redox couple suggests that **1** and **1**$^+$ are described as $[Mo_2^{III}Mo^{IV}Fe^{II}S_4]^{4+}$ and $[Mo_2^{III}Mo^{IV}Fe^{III}S_4]^{5+}$, respectively, and the redox event is largely confined to the Fe site and cycle through Fe(II) Fe(III) oxidation state. (v) The intimate redox description of $Mo_3(FeCl)S_4(dmpe)_3Cl_3$ (**1**) (formally $[Mo_2^{III}Mo^{IV}Fe^{II}S_4]^{4+}$) has implications for its synthesis, as it is prepared from $[Mo_3S_4(dmpe)_3Cl_3]^+$ (formally $[Mo_3^{IV}S_4]^{4+}$) cluster via addition of $FeCl_2$ in the presence of a reductor. Hence, two-electron reduction of the starting $[Mo_3S_4(dmpe)_3Cl_3]^+$ complex, rather than $FeCl_2$ reduction, seems to be the driving force of iron incorporation.

■ ASSOCIATED CONTENT

Ⓢ Supporting Information

ROB3LYP calculated atomic contributions to the molecular orbitals of compound **1** (Table S1). Magnetic susceptibility measurements for **2**−**4** (Figure S1) and X-band EPR spectra of a powder sample of **1** and **1**/[**1**]PF_6 at different temperatures and X-band EPR (Figures S2 and S3) spectra for **2** and **3** (Figure S4). Cyclic voltammograms in the 1.5 to 0 V range for **1**−**4** (Figure S5). Crystallographic data (excluding structure factors) for the structures reported in this paper. This material is available free of charge via the Internet at http://pubs.acs.org.

■ AUTHOR INFORMATION

Corresponding Author

*Tel: +34 964728086. Fax: +34 964728066. E-mail: rosa.llusar@uji.es (R.L.). Tel: +34 964387344. Fax: +34 964387309. E-mail: barrera@sg.uji.es (C.V.).

Notes

The authors declare no competing financial interest.

■ ACKNOWLEDGMENTS

This work was supported by the Spanish Ministerio de Ciencia e Innovación (MICINN) (Projects CTQ2008-02670, CTQ2010-15364, and CSD2007-00010), Spanish Ministerio de Economia y Competitividad (Grant CTQ2011-23157) Fundació Bancaixa-UJI (Projects P1.1B2010-46), ARAID, Ibercaja grant for young researchers (Spain), and Generalitat Valenciana (Projects ACOMP2011-037, ACOMP2011-108, PROMETEO/2009/053, and PROMETEO/2009/108). I.S. thanks the MICINN for a doctoral fellowship (FPU). We are also grateful to the Serveis Centrals d'Instrumentació Científica (SCIC) of the Universitat Jaume I for providing us with mass spectrometry and X-ray facilities.

■ REFERENCES

(1) (a) Holm, R. H.; Kennepohl, P.; Solomon, E. I. *Chem. Rev.* **1996**, *96*, 2239. (b) Lee, S. C.; Holm, R. H. *Chem. Rev.* **2004**, *104*, 1135.

(2) (a) Coucouvanis, D.; Mosier, P. E.; Demadis, K. D.; Patton, S.; Malinak, S. M.; Kim, C. G.; Tyson, M. A. *J. Am. Chem. Soc.* **1993**, *115*, 12193. (b) Demadis, D. K.; Coucouvanis, D. *Inorg. Chem.* **1994**, *33*, 4195. (c) Demadis, D. K.; Coucouvanis, D. *Inorg. Chem.* **1995**, *34*, 436. (d) Laughlin, L. J.; Coucouvanis, D. *J. Am. Chem. Soc.* **1995**, *117*, 3118. (e) Demadis, D. K.; Malinak, S. M.; Coucouvanis, D. *Inorg. Chem.* **1996**, *35*, 4038. (f) Malinak, S. M.; Simeonov, A. M.; Mosier, P. E.; McKenna, C. E.; Coucouvanis, D. *J. Am. Chem. Soc.* **1997**, *119*, 1662.

(3) (a) Beinert, H.; Holm, R. H.; Munck, E. *Science* **1997**, *277*, 653. (b) Einsle, O.; Tezcan, F. A.; Andrade, S. L. A; Schmid, B.; Yoshida, M.; Howard, J. B.; Rees, D. C. *Science* **2002**, *297*, 1696. (c) Evans, D. J.; Pickett, C. J. *Chem. Soc. Rev.* **2003**, *32*, 268.

(4) (a) Hidai, M.; Kuwata, S.; Mizobe, Y. *Acc. Chem. Res.* **2000**, *33*, 46. (b) Llusar, R.; Uriel, S. *Eur. J. Inorg. Chem.* **2003**, 1271. (c) Seino, H.; Hidai, M. *Chem. Sci.* **2011**, *2*, 847.

(5) Feliz, M.; Llusar, R.; Uriel, S.; Vicent, C.; Brorson, M.; Herbst, K. *Polyhedron* **2005**, *24*, 1212.

(6) (a) Feliz, M.; Guillamon, E.; Llusar, R.; Vicent, C.; Stiriba, S. E.; Perez-Prieto, J.; Barberis, M. *Chem.—Eur. J.* **2006**, *12*, 1486. (b) Guillamon, E.; Llusar, R.; Perez-Prieto, J.; Stiriba, S. E. *J. Organomet. Chem.* **2008**, *693*, 1723.

(7) Feliz, M.; Garriga, J. M.; Llusar, R.; Uriel, S.; Humphrey, M. G.; Lucas, N. T.; Samoc, M.; Luther-Davies, B. *Inorg. Chem.* **2001**, *40*, 6132.

(8) Feliz, M.; Llusar, R.; Uriel, S.; Vicent, C.; Coronado, E.; Gómez-Garcia, C. *Chem.—Eur. J.* **2004**, *10*, 4308.

(9) Algarra, A. G.; Basallote, M. G.; Fernandez-Trujillo, M. J.; Llusar, R.; Pino-Chamorro, J. A.; Sorribes, I.; Vicent, C. *Dalton Trans.* **2010**, *39*, 3725.

(10) Shibahara, T.; Sakane, G.; Naruse, Y.; Taya, K.; Akashi, H.; Ichimura, A.; Adachi, H. *Bull. Chem. Soc. Jpn.* **1995**, *68*, 2769.

(11) Shibahara, T.; Akashi, H.; Kuroya, H. *J. Am. Chem. Soc.* **1986**, *108*, 1342.

(12) Yamauchi, T.; Takagi, H.; Shibahara, T.; Akashi, H. *Inorg. Chem.* **2006**, *45*, 5429.

(13) Curtis, M. D.; Riaz, U.; Curnow, O. J.; Kampf, J. W. *Organometallics* **1995**, *14*, 5337.

(14) Hernandez-Molina, R.; Kalinina, I.; Sokolov, M. N.; Peris, G.; Llusar, R. *Synth. React. Inorg., Mech.* **2007**, *37*, 765.

(15) (a) Dreizler, R. M.; Gross, E. K. U. *Density Functional Theory*; Springer-Berlag: Berlin, 1990. (b) Parr, R.; Yang, W. *Density-Functional Theory of Atoms and Molecules*; Oxford University Press: New York, 1989.

(16) Vasco-Rodrigues, J.; Santos, I. C.; Gama, V.; Henriques, R. T.; Waerenborgh, J. C.; Duarte, M. T.; Almeida, M. *J. Chem. Soc., Dalton Trans.* **1994**, 2655.

(17) (a) *SAINT*, v. 5.0.; Bruker Analytical X-Ray Systems: Madison, WI, 1996. (b) Sheldrick, G. M. *SADABS Empirical Absorption Program*; University of Göttingen: Germany, 1996.

(18) Sheldrick, G. M. *SHELXTL*, v. 5.1; Bruker Analytical X-Ray Systems: Madison, WI, 1997.

(19) Frisch, M. J.; Trucks, G. W.; Schlegel, H. B.; Scuseria, G. E.; Robb, M. A.; Cheeseman, J. R.; Scalmani, G.; Barone, V.; Mennucci, B.; Petersson, G. A.; Nakatsuji, H.; Caricato, M.; Li, X.; Hratchian, H. P.; Izmaylov, A. F.; Bloino, J.; Zheng, G.; Sonnenberg, J. L.; Hada, M.; Ehara, M.; Toyota, K.; Fukuda, R.; Hasegawa, J.; Ishida, M.; Nakajima, T.; Honda, Y.; Kitao, O.; Nakai, H.; Vreven, T.; Montgomery, J. A., Jr.; Peralta, J. E.; Ogliaro, F.; Bearpark, M.; Heyd, J. J.; Brothers, E.; Kudin, K. N.; Staroverov, V. N.; Kobayashi, R.; Normand, J.; Raghavachari, K.; Rendell, A.; Burant, J. C.; Iyengar, S. S.; Tomasi, J.; Cossi, M.; Rega, N.; Millam, J. M.; Klene, M.; Knox, J. E.; Cross, J. B.; Bakken, V.; Adamo, C.; Jaramillo, J.; Gomperts, R.; Stratmann, R. E.; Yazyev, O.; Austin, A. J.; Cammi, R.; Pomelli, C.; Ochterski, J. W.; Martin, R. L.; Morokuma, K.; Zakrzewski, V. G.; Voth, G. A.; Salvador, P.; Dannenberg, J. J.; Dapprich, S.; Daniels, A. D.; Farkas, O.; Foresman, J. B.; Ortiz, J. V.; Cioslowski, J.; Fox, D. J. *Gaussian 09*, revision A.01; Gaussian, Inc.: Wallingford, CT, 2009.

(20) (a) Lee, C.; Parr, R. G.; Yang, W. *Phys. Rev. B* **1988**, *37*, B785. (b) Becke, A. D. *J. Phys. Chem.* **1993**, *98*, 64.

(21) Zhang, Y. P.; Bashkin, J. K.; Holm, R. H. *Inorg. Chem.* **1987**, *26*, 694.

(22) Guillamon, E.; Llusar, R.; Pozo, O.; Vicent, C. *Int. J. Mass Spectrom.* **2006**, *254*, 28.

(23) (a) Scott, T. A.; Berlinguette, C. P.; Holm, R. H.; Zhou, H. C. *Proc. Natl. Acad. Sci. U.S.A.* **2005**, *102*, 9741. (b) Russell, P.; Pesavento, P.; Berlinguette, C. P.; Holm, R., H. *Inorg. Chem.* **2007**, *46*, 510.

(24) Llusar, R.; Sorribes, I.; Vicent, C. *Inorg. Chem.* **2009**, *48*, 4837.

(25) Bahn, C. S.; Tan, A.; Harris, S. *Inorg. Chem.* **1998**, *37*, 2770.

(26) Alberola, A.; Polo, V.; Gomez-Garcia, C.; Andres, J.; Llusar, R.; Vicent, C. *Inorg. Chem.* **2008**, *47*, 3661.

(27) Mabbs, F. E.; Collison, D. *Electron Paramagnetic Resonance of d Transition Metal Compounds*; Elsevier Science Publishers B. V.: Amsterdam, 1992; pp 548−579.

(28) (a) Katada, M.; Akashi, H.; Shibahara, T.; Sano, H. *J. Radioanal. Nucl. Chem. Lett.* **1990**, *145*, 143. (b) Dimmock, P. W.; Dickson, D. P. E.; Sykes, A. G. *Inorg. Chem.* **1990**, *29*, 5120.

(29) Greenwood, N. N.; Gibb, T. C. *Mössbauer Spectroscopy*, 1st ed.; Chapman and Hall, Ltd. Publishers: London, 1971.

(30) Hauser, C.; Bill, E.; Holm, R. H. *Inorg. Chem.* **2002**, *41*, 1615.

(31) Cen, W.; Lee, S. C.; Li, J.; MacDonnell, F. M.; Holm, R. H. *J. Am. Chem. Soc.* **1993**, *115*, 9515.

(32) (a) Goh, C.; Segal, B. M.; Huang, J.; Long, J. R.; Holm, R. H. *J. Am. Chem. Soc.* **1996**, *118*, 11844. (b) Osterloh, F.; Segal, B. M.; Achim, C.; Holm, R. H. *Inorg. Chem.* **2000**, *39*, 980. (c) Zhou, C.; Holm, R. H. *Inorg. Chem.* **2003**, *42*, 11.